Available online at www.sciencedirect.com

ScienceDirect

Energy Procedia 97 (2016) 302 – 309

Energy Procedia

European Geosciences Union General Assembly 2016, EGU
Division Energy, Resources & Environment, ERE

Gas hydrate stability zone of the Barents Sea and Kara Sea region

Peter Klitzke[a,b,*], Manja Luzi-Helbing[a], Judith M. Schicks[a], Mauro Cacace[a], Antoine B. Jacquey[a,b], Judith Sippel[a], Magdalena Scheck-Wenderoth[a,b], Jan Inge Faleide[c,d]

[a] GFZ German Research Centre for Geosciences, Potsdam, Germany
[b] RWTH Aachen University, Department of Geology, Geochemistry of Petroleum and Coal, Aachen, Germany
[c] Centre for Earth Evolution and Dynamics (CEED), Department of Geosciences, University of Oslo, Oslo, Norway
[d] Research Centre for Arctic Petroleum Exploration (ARCEx) University of Tromsø, Tromsø, Norway

Abstract

In this study we assess the present-day gas hydrate stability zone for the Barents Sea and Kara Sea region. Thereby, we make use of a data-based 3D lithosphere-scale pressure and thermal model. The resulting gas hydrate stability zone varies within >1 km across the study area and strongly correlates with the local geological settings and the corresponding geothermal gradient. Gas hydrates containing hydrocarbons from a thermogenic source (CH_4+C_2H_3+C_3H_8) are potentially more widespread than previously assumed. The corresponding thermogenic feed gas may have derived from leaking petroleum systems during late Cenozoic basin inversion.

Peer-review under responsibility of the organizing committee of the General Assembly of the European Geosciences Union (EGU)

Keywords: gas hydrate stability zone; 3D modelling, Barents Sea and Kara Sea

1. Introduction

Natural gas hydrates occur widely along continental margins and in permafrost regions where favourable low-temperature and high-pressure conditions exist. Their distribution critically depends on the supply and composition of a feed gas. The most common component is methane, a gas with a global warming potential 25 times stronger than carbon dioxide within 100 years [1]. Generally, the feed gas is considered to derive from shallow microbial sources (methane content: >99%) or as thermogenic gas from deeper leaked petroleum systems (methane content: 25-99%) [2]. Recently, an abiotic methane from mantle serpentinisation has also been proposed as potential source [3,4].

* Corresponding author. Tel.: +49-331-288-2846; fax: +49-331-288-1349.
E-mail address: klitzke@gfz-potsdam.de

Peer-review under responsibility of the organizing committee of the General Assembly of the European Geosciences Union (EGU)
doi:10.1016/j.egypro.2016.10.005

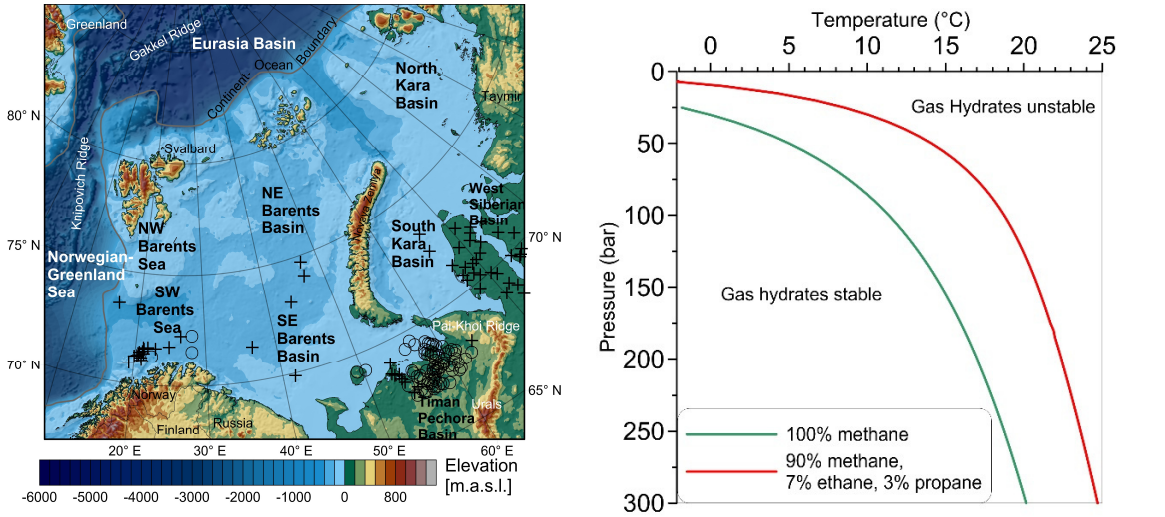

Fig. 1: (a) Bathymetry and topography [57] of the petroliferous Barents Sea and Kara Sea region. Crosses and circles mark the position of gas and oil fields, respectively [58]; (b) Pressure and temperature stability conditions for gas hydrates formed from two different feed gas compositions and 3.5% pore water salinity.

One method to identify submarine gas hydrate occurrences is the interpretation of bottom simulating reflectors in seismic data. [e.g. 5]. A bottom-simulating reflector is the result of an impedance contrast between the base of the hydrate-saturated sediments above and free gas in the sediments below. The absence of a bottom-simulating reflector, however, does not exclude the occurrence of gas hydrates but may be explained by a lower degree of hydrate saturation or the absence of free gas below the gas hydrate stability zone [6,7]. In this sense, geophysical methods may completely underestimate the distribution of gas hydrates.

Bottom-simulating reflectors have been interpreted at several sites west of Svalbard and in the SW Barents Sea [e.g. 8–14]. It is widely discussed that the gas hydrates are fed by leaking petroleum systems in response to late Cenozoic uplift and glacial erosion [15–17]. Potential pathways are well described for the SW Barents Sea where a dense geological and geophysical database exists. Recent findings of gas hydrates and evidences for fluid flow in the eastern Barents Sea [18] and in the southern Kara Sea [19] suggest that gas hydrates may occur more widespread than previously assumed.

The potential gas hydrate stability field of the entire Barents Sea and Kara Sea region has been investigated only by a few studies so far [e.g. 20]. These studies cover the entire Arctic or even the global scale and simplify the local geological complexity and the corresponding physical parameterisation of their models. Due to phases of Cenozoic uplift and erosion the sedimentary units of the Barents Sea and Kara Sea region have significantly lower porosities than expected according to their present-day burial depth [15–17]. Laterally varying porosities directly influence the thermal conductivity, the thermal field and hence should be considered when assessing the thickness of the gas hydrate stability zone.

In the frame of this study, we make use of an existing 3D structural-thermal model which reproduces the lithosphere-scale geological and physical complexity of the Barents Sea and Kara Sea region (Fig. 1a) [21,22]. We want to address in particular two leading questions: Where are gas hydrates of a defined composition potentially stable at present-day? How does the thermal state, as derived from the geological setting, control the gas hydrate stability?

2. Model and methods

Gas hydrates are inclusion compounds commonly composed of water and gas. Natural gas hydrates contain predominantly methane but they may also encase other gases resulting in a mixed gas hydrate. Higher amounts of e.g. ethane, propane, carbon dioxide and hydrogen sulphide besides methane increase the gas hydrate stability with respect to temperature and pressure conditions [23]. To predict the gas hydrate phase boundaries the CSMGem software [24] is employed which considers the feed gas composition, the pressure and temperature conditions and the pore water salinity. Figure 1b shows the calculated stability fields for two different feed gas compositions: a biogenic pure

methane feed gas and a thermogenic feed gas (90% methane; 7% ethane, 3% propane) which was recently described for the SW Barents Sea [13].

We obtain the 3D temperature and pressure configuration of the lithosphere below the Barents Sea and Kara Sea region based on a 3D structural model [21,22]. The model has a horizontal resolution of 10 km and resolves vertically five sedimentary units, the continental upper and lower crust, the oceanic crust and the lithospheric mantle. Each geological unit is characterised by lithology-dependent mechanical and thermal parameters such as porosity, density, radiogenic heat production and the matrix thermal conductivity (Table 1). For the sedimentary units, usual porosity-depth curves are inapplicable due to late Cenozoic episodes of uplift and erosion. Therefore, we account for the additional load from the eroded geological units by introducing an artificial layer on top of the model to calculate the maximum-burial dependent porosity (Φ_z) with the lithology-dependent surface porosity (Φ_0) and the compaction coefficient (c) (Table 1).

(1) $$\Phi_z = \Phi_0 * e^{-cz}$$

The resulting porosity configuration is used to determine the spatial distribution of sedimentary bulk densities (ρ_b) using the weighted geometric mean equation with the depth-dependent porosity (ϕ_z), the density of liquid water (1024 kg/m³; ρ_w) assumed to fill the pore space and the matrix density of the solid rock components (ρ_s).

(2) $$\rho_b = \rho_w^{\phi_z} * \rho_s^{(1-\phi_z)}$$

Subsequently, the pressure is calculated at each grid node with ρ_b the bulk density, g the gravitational acceleration and z the depth. Thereby, the hydrostatic as well as the lithostatic pressures are considered.

(3) $$\nabla P = \rho_b * g * \nabla z$$

We determine the 3D thermal field by assuming heat conduction as the dominant heat transport mechanism on the scale of the lithosphere. This is expressed by the steady-state equation with λ_b the bulk thermal conductivity and H the radiogenic heat generation.

(4) $$H = \nabla \cdot (\lambda_b \nabla T)$$

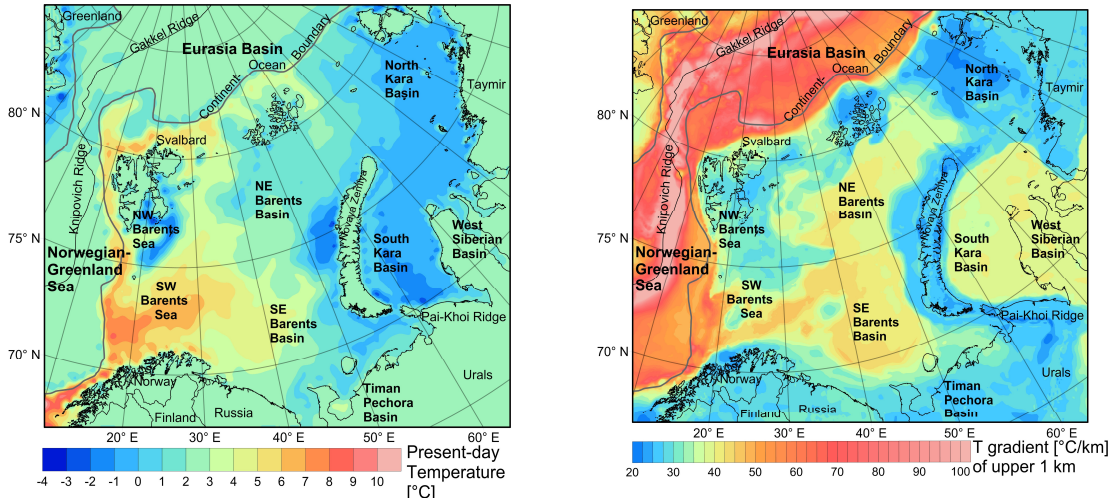

Fig. 2. (a) Present-day temperature distribution at the seafloor [28]; (b) Geothermal gradient of the uppermost 1 km below the topography.

Governing equations for the mechanical load (3) and conductive 3D thermal field (4) have been integrated in a massively parallel finite-element-method based framework (MOOSE). The MOOSE framework provides a powerful and flexible platform to solve multiphysics problems implicitly on unstructured meshes [25].

The steady-state heat equation (4) is sensitive to the assigned thermal properties (thermal conductivity, radiogenic heat production; Table 1) as well as to the choice of boundary conditions. The reduced present-day porosities of shallow sediments as a consequence of Cenozoic uplift and erosion result in higher thermal conductivities of the sediments than would be expected given their actual burial depth (Table 1).

For the lower thermal boundary we assign 1300°C at the base of the lithosphere. This interface corresponds to a zone where shear wave velocities are decreasing with increasing depth [21,26,27] which is interpreted as first partial melting of peridotite at a temperature of ~1300°C and hence, as transition between lithospheric and asthenospheric mantle. The depth of the lithosphere-asthenosphere boundary is shallowest in the oceanic domain and increasing below the continental domain from the western Barents Sea (~110 km) to the central and eastern Barents Sea (~150 km) and to the Kara Sea (~200 km) [22].

The upper boundary is defined by seafloor temperatures extracted from the MPI-ESM-MR climate model [28] (Fig. 2a). Highest present-day seafloor temperatures occur in the western Barents Sea (~8°C) due to the inflow of warm water masses from the North Atlantic. Towards the east, temperatures are decreasing gradually down to -2°C in the southern Kara Sea.

Finally, we extract the potential gas hydrate stability zone by comparing the pressure and temperature at each grid node with the gas hydrates stability conditions obtained from the CSMGem software.

Table 1. Mechanical and thermal properties of geological units. BARMOD represents a 3D density dataset was assigned to the upper mantle.

Megasequences	**Modelled lithology***	**Surface porosity Φ_0**	**Compaction coefficient k (km^{-1})**	**Calculated average bulk density (kg m^3)**	**Avg. bulk thermal conductivity λ ($W\ m^{-1}\ K^{-1}$)**	**Radiogen. heat production S ($\mu W\ m^{-3}$)**
Earliest Eocene - Present	25% SS 75% SH	0.63	0.7	2200	1.48	1.3
M.Cret - Paleocene	10% SS 90% SH	0.67	0.8	2500	1.62	1.4
M.Jurassic - M.Cret	10% SS 90% SH	0.67	0.8	2600	1.71	1.4
M.Permian - M.Jurassic	50% SS 40% SH 10% LS	0.54	0.5	2650	2.54	1.1
Pre-mid-Permian	40% SS 10% SH 25% LS 25% DOL	0.46	0.4	2650	2.95	0.7
*SH-shale, SS – sandstone, LS – limestone, DOL - dolomite						
Subsedimentary Geological Units		Density (kg m^3)			Thermal conductivity ($W\ m^{-1}\ K^{-1}$)	Radiogenic heat prod. ($\mu W\ m^{-3}$)
Crystalline Crust	**Cont. Upper Crust**	2750			2.7	1.7
	Cont. Lower Crust	3020			2.5	0.5
	High-density body	3300			2.6	0.3
	Oceanic Crust	2920			2.3	0.3
Lithospheric Mantle	**Continent**	BARMOD (beyond: 3320)			4	0.01

3. Results

The thickness of the potential gas hydrate stability zone varies within >1 km across the Barents Sea and Kara Sea region. In the oceanic domain, methane hydrates reach an average thickness of ~200-300 m (Fig. 3a). Thereby, the methane hydrate thickness distribution reveals a significant correlation with the age and the thickness of the oceanic

lithosphere. Thickness maxima of up to 600 m are restricted to the thick sedimentary fans along the continental margin. These fans formed in response to late Cenozoic uplift and glacial erosion and represent the oldest part of the oceanic domain. Accordingly, they are underlain by the thickest oceanic lithosphere (50 km) and characterised by a rather low geothermal gradient (~45-50°C/km; Fig. 2b). Towards the Knipovich and Gakkel mid oceanic ridges, the gas hydrate stability zone pinches out due to gradually increasing geothermal gradient (>120°C/km) and the absence of sediments. The thickness of the gas hydrate stability field increases by ~130 m along the continental margin for a thermogenic feed gas (Fig. 3b).

A biogenic pure methane hydrate is only locally stable in the continental domain where sufficient water depths or a low geothermal gradients exists such as in the areas next to Novaya Zemlya, the troughs along the northern continental margin and in the northern Kara Sea region (Fig. 3a). In addition, methane hydrates are locally stable in the central, eastern Barents Sea and in the Timan Pechora Basin with thickness of 100 to 300 m (Fig. 3a). In contrast, a mixed gas hydrate formed from thermogenic gas sources (feed gas composition: 90% methane, 7% ethane and 3% propane) is potentially stable across wide parts of the study area (Fig. 3b). Thickness maxima (>1 km) occur in the northern Kara Sea, Franz Josef Land, Svalbard and the troughs west and east of Novaya Zemlya [21,22]. These regions are characterised by low geothermal gradients (~25°C/km; Fig. 2b) due to a thick underlying lithosphere and/or the wide absence of young insulating sediments. In the remaining shelf region the thickness of the stability zone varies between 200 m and 550 m such as the eastern Barents Sea and the southern Kara Sea. These regions are characterised by similar shallow water depths (~200 m to 300 m), so that not surprisingly, the local geothermal gradient (~35-40°C/km) controls local thickness variations of the modelled gas hydrate stability zone (Figs. 2b, 3).

4. Discussions

4.1. Oceanic Domain/ western Svalbard

Seismic profiles reveal numerous bottom-simulating reflectors along the continental margin west of Svalbard [e.g. 8,10,12]. Geissler et al. (2014) mapped a bottom-simulating reflectors across wide parts of the margins between latitude 79° and 82° (Fig. 3c). The interpreted gas hydrates show reveal a patchy distribution with strongly varying thickness of several hundred meters which may point to locally differing gas sources. This is further supported by measurements of gas emissions which suggest microbial [29–31] as well as thermogenic gas origins [29,32]. Interpreted bottom-simulating reflectors at average depths of 200 m to 300 m coincide with modelling results for a pure methane hydrate composition. Locally, bottom-simulating reflectors show depth anomalies of more than 400 m. These depths rather correspond to the modelled thermogenic gas hydrate compositions.

A potential thermogenic feeding system might be an Early to Middle Eocene source rock interpreted recently across the Lomonosov Ridge [33–35]. This source rock is not sufficiently deep across the Lomonosov Ridge to produce hydrocarbons. Nevertheless, seismic lines imply increasing depositional depths towards the Armundsen Basin so that burial depths may be sufficient to generate hydrocarbons in the deeper Arctic Basins. However, according to the inferred oceanic age, Early to Middle Eocene sediments would be restricted to the margins of the Eurasia Basin and to the southern Norwegian Greenland Sea within the study area. The Fram Strait, which characterises the region west of Svalbard, did not open before Miocene times and thus, after the deposition of the potential source rocks [36]. An alternative potential source rock is of Miocene age and was drilled at ODP leg 151 Hole 909c west of Svalbard [37]. Though this source rock is described as immature to marginal mature [38] it has been recently proposed that the rapid burial of the Miocene source rock and elevated heat flow due to seafloor spreading are sufficient to generate hydrocarbons [39]. Another potential gas source in the oceanic domain might be serpentinisation processes typically occurring at mid-oceanic ridges where lithospheric mantle is exposed to sea water [3,4]. Fluid-rock interactions between sea water and the upper mantle result in the metamorphism of peridotite whereby abiogenic methane is formed potentially feeding gas hydrates. Rajan et al. (2012) interpreted a bottom-simulating reflector overlying a serpentinised basement segment which supports this scenario [40,41]. In contrast, geochemical analysis from gas hydrates in vicinity of the Vestnesa Ridge west of Svalbard reveal a light $\delta^{13}C$ composition which would exclude a mantle source [32].

4.2. SW Barents Sea

Though the SW Barents Sea is characterised by a shallower bathymetry (<450 m), interpreted bottom-simulating reflectors are at similar depths (~220 to ~345 m) compared to the western Svalbard area (cf. >1000 m) [9,13,42–44]. This is partly related to a generally lower geothermal gradient in the SW Barents Sea (~30-60°C/km; cf. 70-120°C western Svalbard; Fig. 2b) and inferred mixed hydrates with a larger stability field [e.g. 42]. This is in line with our modelling results which reveal that a pure methane hydrate is unstable in the SW Barents Sea (Fig. 3a). Instead, the best fit with the interpreted depth to bottom-simulating reflectors is achieved with a mixed feed gas composition of 90% methane, 7% ethane and 3% propane (Fig. 3b) which fits the chemical composition of the Snøhvit gas field [13]. In contrast, a feed gas with lower amounts of heavy hydrocarbons (3% ethane; 1% propane) reproduces the inferred base of the gas hydrate stability zone at 220 m depth below the central Barents Sea [44,45].

Several gas-prone petroleum systems are inferred beneath the SW Barents Sea providing a potential source for mixed gas hydrates (Fig. 1a) [46,47]. Oligocene to Miocene episodes of tectonic uplift and glacial erosion resulted in gas expansion, tilting of reservoirs, seal failure and hydrocarbon leakage [47–49]. In addition, Pliocene/Pleistocene ice sheet coverage involved further erosion which likely reinforced hydrocarbon leakage. During the glacial periods, permafrost may have acted as a seal for the rising gases and the additional load of the ice sheets may have triggered the formation of gas hydrates from the trapped gas. Ostanin et al. (2013) estimate thickness of 600 m for thermogenic hydrates during the last glacial maximum. The modelled present-day thickness of ~200 m indicate that the stability zone for thermogenic hydrates thinned by ~400 m following the retreat of the ice sheet and corresponding pressure release. The released fluids reached the surface and formed the widely observed pockmarks (Fig. 3c) [12,50–52]. At present-day, these pockmarks of the SW Barents Sea are assumed to be widely inactive [50,51]. Gas flares mapped by seismic data suggest that present-day fluid flow is restricted to open fault systems [52].

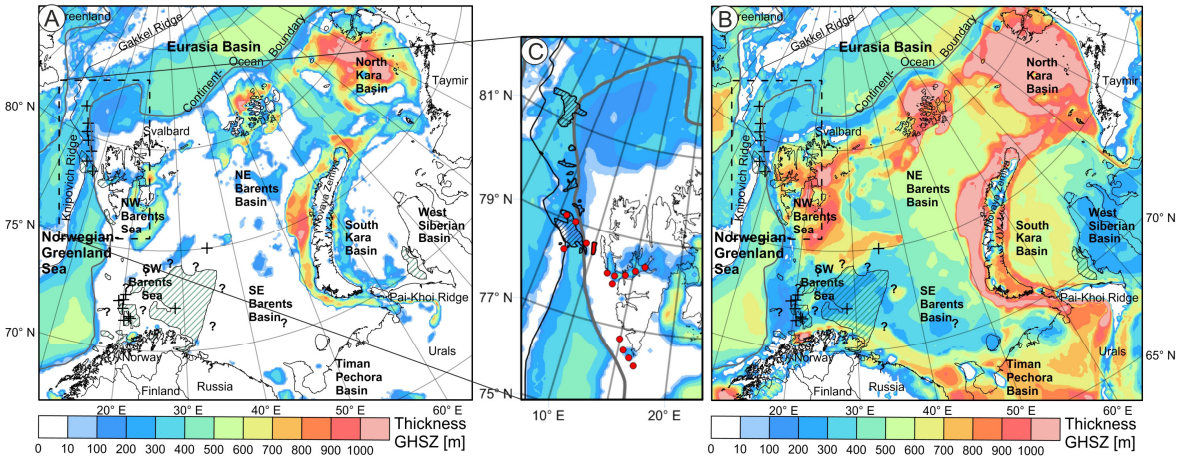

Fig. 3. (a) Thickness of the gas hydrate stability zone for a pure methane hydrate and (b) a thermogenic feed gas composition composed of 90% methane, 7% ethane and 3% propane. Interpreted gas hydrates are marked with a cross. The distribution of pockmarks and gas flares is marked with striped polygons; (c) A magnification of the Svalbard region. The polygon delineates the distribution of gas hydrates and the red dots characterise regions where pockmarks and gas flares are described (see text for references).

4.3. Remaining continental domain of the study area

Petroleum systems are inferred for all major sedimentary basins beyond the SW Barents Sea such as the Kara Sea and the eastern Barents Sea [34,35,37,47,53,54]. Likewise, these basins experienced late Cenozoic inversion and glacial erosion including most likely hydrocarbon leakage [13,15–17,49]. Our modelling results reveal that released thermogenic fluids would find stable pressure and temperature conditions over wide parts of the study area (Fig. 3b). In fact, there are a few studies which describe evidences for fluid flow such as gas flares and pockmarks in the SE Barents Sea [18], the central Barents Sea [45] and the southern Kara Sea [19,55], though the data coverage is generally very sparse for these remote regions. Recent measurements of gas flares in the southern Kara Sea indicate a biogenic

gas origin released from thawing permafrost [55,56]. The presence of permafrost suggest that some offshore regions may have not reached thermal steady-state at present-day following the last glacial maximum. Accordingly, the shallow subsurface might be locally colder than predicted by the presented thermal model.

5. Conclusion

In summary, we assess the gas hydrate inventory of the Barents Sea and Kara Sea region for two different feed gas compositions. The modelled potential gas hydrate stability zone varies significantly across the study area and strongly depends on the local geological setting, the corresponding geothermal gradient and the feed gas composition. Mixed gas hydrates formed from thermogenic feed gas are potentially stable over wide parts of the study area. The corresponding thermogenic feed gas may have derived from leaking petroleum systems in response to late Cenozoic basin inversion. Accordingly, these mixed gas hydrates may be more widespread than previously assumed. Future studies require more in situ geochemical and geophysical analysis in combination with petroleum system modelling to further assess the formation and dissolution of gas hydrates through time and space. Nevertheless, this study presents a first valuable insights into the potential gas hydrate inventory of a geological complex region.

References

[1] Forster P, Artaxo P, Lowe DC, Raga G. Changes in Atmospheric Constituents and in Radiative Forcing. In: Clim. Chang. 2007 Phys. Sci. basis. Contrib. Work. Gr. I to Fourth Assess. Rep. Intergov. Panel Clim. Chang., Cambridge, UK: Cambridge Press; 2007, p. 129–234.
[2] Kvenvolden KA. A review of the geochemistry of methane in natural gas hydrate. Org Geochem 1995;23:997–1008.
[3] Johnson JE, Mienert J, Plaza-Faverola A, Vadakkepuliyambatta S, Knies J, Bunz S, et al. Abiotic methane from ultraslow-spreading ridges can charge Arctic gas hydrates. Geology 2015;43:371–4.
[4] Rajan A, Mienert J, Bünz S, Chand S. Potential serpentinization, degassing, and gas hydrate formation at a young (<20 Ma) sedimented ocean crust of the Arctic Ocean ridge system. J Geophys Res Solid Earth 2012;117:1-14.
[5] Shipley TH, Houston MH. Seismic Evidence for Widespread Possible Gas Hydrate Horizons on Continental Slopes and Rises. Am Assoc Pet Geol Bull 1979;63:2204–13.
[6] Chand S, Minshull TA, Gei D, Carcione JM. Elastic velocity models for gas-hydrate-bearing sediments. Geophys J Int 2004;159:573–90.
[7] Vanneste M, De Batist M, Golmshtok A, Kremlev A, Versteeg W. Multi-frequency seismic study of gas hydrate-bearing sediments in Lake Baikal, Siberia. Mar Geol 2001;172:1–21.
[8] Vanneste M, Guidard S, Mienert J. BSR and geothermal gradients across the western Svalbard margin. Terra Nov 2005;17:510–6.
[9] Laberg JS, Andreassen K. Gas hydrate and free gas indications within the Cenozoic succession of the Bjornoya Basin, western Barents Sea. Mar Pet Geol 1996;13:921–40.
[10] Geissler WH, Pulm P V, Jokat W, Gebhardt a C. Indications for the Occurrence of Gas Hydrates in the Fram Strait from Heat Flow and Multichannel Seismic Reflection Data. J Geophys Res 2014;2014. d
[11] Bünz S, Polyanov S, Vadakkepuliyambatta S, Consolaro C, Mienert J. Active gas venting through hydrate-bearing sediments on the Vestnesa Ridge, offshore W-Svalbard. Mar Geol 2012;332–334:189–97.
[12] Chand S, Mienert J, Andreassen K, Knies J, Plassen L, Fotland B. Gas hydrate stability zone modelling in areas of salt tectonics and pockmarks of the Barents Sea suggests an active hydrocarbon venting system. Mar Pet Geol 2008;25:625–36.
[13] Ostanin I, Anka Z, di Primio R, Bernal A. Hydrocarbon plumbing systems above the Snøhvit gas field: Structural control and implications for thermogenic methane leakage in the Hammerfest Basin, SW Barents Sea. Mar Pet Geol 2013;43:127–46.
[14] Rajan A. Geophysical characterizations of fluid flow and gas-hydrate systems of the NW-Svalbard and SW-Barents Sea margins. UNIVERSITY OF TROMSØ, 2012.
[15] Dimakis P, Braathen BI, Faleide JI, Elverhøi A, Gudlaugsson ST. Cenozoic erosion and the preglacial uplift of the Svalbard–Barents Sea region. Tectonophysics 1998;300:311–27.
[16] Sobolev P. Cenozoic uplift and erosion of the Eastern Barents Sea – constraints from offshore well data and the implication for petroleum system modelling. Zeitschrift Der Dtsch Gesellschaft Für Geowissenschaften 2012;163:309–24.
[17] Henriksen E, Bjornseth HM, Hals TK, Heide T, Kiryukhina T, Klovjan OS, et al. Chapter 17 Uplift and erosion of the greater Barents Sea: impact on prospectivity and petroleum systems. Geol Soc London, Mem 2011;35:271–81.
[18] Lein AY, Nemirovskaya IA, Ivanov M V. Isotope composition of organic and carbonate carbon of surface horizons of bottom sediments in the area of the Shtokmanovskoe deposit and “pockmarks field” in the Barents Sea. Dokl Earth Sci 2012;446:1067–70.
[19] Portnov A, Smith AJ, Mienert J, Cherkashov G, Rekant P, Semenov P, et al. Offshore permafrost decay and massive seabed methane escape in water depths >20 m at the South Kara Sea shelf. Geophys Res Lett 2013;40:3962–7.
[20] Kretschmer K, Biastoch A, Rupke L, Burwicz E. Modelling the fate of methane hydrates under global warming. Glob Biogeochem Cycles 2015;29:610–25.
[21] Klitzke P, Faleide JI, Scheck-Wenderoth M, Sippel J. A lithosphere-scale structural model of the Barents Sea and Kara Sea region. Solid Earth 2015;6:153–72.
[22] Klitzke P, Sippel J, Faleide JI, Scheck-Wenderoth M. A 3D gravity & thermal model for the Barents Sea and Kara Sea. Tectoph. 2016:1–31.

[23] Schicks JM, Luzi-Helbing M. Kinetic and Thermodynamic Aspects of Clathrate Hydrate Nucleation and Growth. J Chem Eng Data 2014:141201153738006.
[24] Sloan ED, Koh C. Authors. Clathrate Hydrates Nat. Gases, Third Ed. 3rd ed., CRC Press; 2007, p. 752..
[25] Gaston D, Newman C, Hansen G, Lebrun-Grandié D. MOOSE: A parallel computational framework for coupled systems of nonlinear equations. Nucl Eng Des 2009;239:1768–78.
[26] Ritzmann O, Faleide JI. The crust and mantle lithosphere in the Barents Sea/Kara Sea region. Tectonophysics 2009;470:89–104.
[27] Levshin AL, Schweitzer J, Weidle C, Shapiro NM, Ritzwoller MH. Surface wave tomography of the Barents Sea and surrounding regions. Geophys J Int 2007;170:441–59.
[28] Giorgetta MA, Jungclaus JH, Reick CH, Legutke S, Bader J, Böttinger M, et al. Climate and carbon cycle changes from 1850 to 2100 in MPI-ESM simulations for the coupled model intercomparison project phase 5. J Adv Model Earth Syst 2013;5:572–97.
[29] Knies J, Damm E, Gutt J, Mann U, Pinturier L. Near-surface hydrocarbon anomalies in shelf sediments off Spitsbergen: Evidences for past seepages. Geochemistry, Geophys Geosystems 2004;5.
[30] Fisher RE, Sriskantharajah S, Lowry D. Arctic methane sources: Isotopic evidence for atmospheric inputs. Geophys Res Lett 2011;38.
[31] Sahling H, Römer M, Pape T, Bergès B, Dos Santos Fereirra C, Boelmann J, et al. Gas emissions at the continental margin west of Svalbard: Mapping, sampling, and quantification. Biogeosciences 2014;11:6029–46.
[32] Smith AJ, Mienert J, Bünz S, Greinert J. Thermogenic methane injection via bubble transport into the upper Arctic Ocean from the hydrate-charged Vestnesa Ridge, Svalbard. Geochemistry, Geophys Geosystems 2014;15:1945–59.
[33] Mann U, Knies J, Chand S. Evaluation and modelling of Tertiary source rocks in the central Arctic Ocean. Mar Pet Geol 2009;26:1624–39.
[34] Stein R. U. Cret./l. Tertiary black shales near the North Pole: Organic-carbon origin and source-rock potential. Mar Pet Geol 2007;24:67–73.
[35] Stein R, Boucsein B, Meyer H. Anoxia and high primary production in the Paleogene central Arctic Ocean: First detailed records from Lomonosov Ridge. Geophys Res Lett 2006;33:2–7.
[36] Engen Ø, Faleide JI, Dyreng TK. Opening of the Fram Strait gateway: A review of plate tectonic constraints. Tectonophysics 2008; 51–69.
[37] Myhre AM, Thiede J, Firth JV. Site 909. In: Myhre AM, Thiede J, Firth JV, editors. Proc. Ocean Drill. Program, 151 Initial Reports, vol. 151, Ocean Drilling Program; 1995, p. 301–43.
[38] Knies J, Mann U. Depositional environment and source rock potential of Miocene strata from the central Fram Strait: Introduction of a new computing tool for simulating organic facies variations. Mar Pet Geol 2002;19:811–28.
[39] Dumke I, Burwicz EB, Berndt C, Klaeschen D, Feseker T, Geissler WH, et al. Gas hydrate distribution and hydrocarbon maturation north of the Knipovich Ridge, western Svalbard margin. J Geophys Res B Solid Earth 2016;121:1405–24.
[40] Hermann T, Jokat W. Crustal structures of the Boreas Basin and the Knipovich Ridge, North Atlantic. Geophys J Int 2013;193:1399–414.
[41] Kandilarov A, Landa H, Mjelde R, Pedersen RB, Okino K, Murai Y. Crustal structure of the ultra-slow spreading Knipovich Ridge, North Atlantic, along a presumed ridge segment center. Mar Geophys Res 2010;31:173–95.
[42] Rajan A, Bünz S, Mienert J, Smith AJ. Gas hydrate systems in petroleum provinces of the SW-Barents Sea. Mar Pet Geol 2013;46:92–106.
[43] Vadakkepuliyambatta S, Hornbach MJ, Bünz S, Phrampus BJ. Controls on gas hydrate system evolution in a region of active fluid flow in the SW Barents Sea. Mar Pet Geol 2015;66:861–72.
[44] Løvø V, Elverhøi A, Antonsen P, Solheim A, Butenko G. Submarine permafrost and gas hydrates in the northern Barents Sea. vol. 56. 1990.
[45] Solheim A, Elverhøi A. A pockmark field in the Central Barents Sea; gas from a petrogenic source? Polar Res 1985;3:11–9.
[46] Cavanagh AJ, Di Primio R, Scheck-Wenderoth M, Horsfield B. Severity and timing of Cenozoic exhumation in the southwestern Barents Sea. J Geol Soc London 2006;163:761–74.
[47] Ohm SE, Karlsen DA, Austin TJF. Geochemically driven exploration models in uplifted areas: Example from the Norwegian Barents Sea. Am Assoc Pet Geol Bull 2008;92:1191–223.
[48] Doré AG, Corcoran D V., Scotchman IC. Prediction of the hydrocarbon system in exhumed basins, and application to the NW European margin. Geol Soc London, Spec Publ 2002;196:401–29.
[49] Doré AG, Jensen LN. The impact of late Cenozoic uplift and erosion on hydrocarbon exploration: offshore Norway and some other uplifted basins. Glob Planet Change 1996;12:415–36.
[50] Nickel JC, di Primio R, Kallmeyer J, Hammer Ø, Horsfield B, Stoddart D, et al. Tracing the origin of thermogenic hydrocarbon signals in pockmarks from the southwestern Barents Sea. Org Geochem 2013;63:73–84.
[51] Rise L, Bellec VK, Chand S, Bøe R. Pockmarks in the southwestern Barents Sea and - Finnmark fjords. Nor J Geol 2015;94:263–82.
[52] Chand S, Thorsnes T, Rise L, Brunstad H, Stoddart D, Bøe R, et al. Multiple episodes of fluid flow in the SW Barents Sea (Loppa High) evidenced by gas flares, pockmarks and gas hydrate accumulation. Earth Planet Sci Lett 2012;331–332:305–14..
[53] Henriksen E, Ryseth AE, Larssen GB, Heide T, Ronning K, Sollid K, et al. Chapter 10 Tectonostratigraphy of the greater Barents Sea: implications for petroleum systems. Geol Soc London, Mem 2011;35:163–95.
[54] Startseva KF, Ershov A V., Nikishin VA. The evolution of hydrocarbon systems in the North Kara sea: Evidence from 2D modeling. Moscow Univ Geol Bull 2015;70:97–106.
[55] Portnov A, Mienert J, Serov P. Modeling the evolution of climate-sensitive Arctic subsea permafrost in regions of extensive gas expulsion at the West Yamal shelf. J Geophys Res G Biogeosciences 2014;119:2082–94.
[56] Serov P, Portnov A, Mienert J, Semenov P, Ilatovskaya P. Methane release from pingo-like features across the South Kara Sea shelf, an area of thawing offshore permafrost. J Geophys Res F Earth Surf 2015;120:1515–29.
[57] Jakobsson M, Mayer L, Coakley B, Dowdeswell JA, Forbes S, Fridman B, et al. The International Bathymetric Chart of the Arctic Ocean (IBCAO) Version 3.0. Geophys Res Lett 2012;39:1–6.
[58] Steinshouer DW, Qiang J, McCabe PJ, Ryder RT. Maps showing geology, oil and gas fields, and geologic provinces of the Asia Pacific region. Version 1. 1997.